

1 The Silicon Vertex Detector of the Belle II Experiment

2 Y. Uematsu^r, K. Adamczyk^u, L. Aggarwal^l, H. Aihara^r, T. Aziz^k, S. Bacher^u,
3 S. Bahinipati^f, G. Batignani^{l,m}, J. Baudot^e, P. K. Behera^g, S. Bettarini^{l,m},
4 T. Bilka^c, A. Bozek^u, F. Buchsteiner^b, G. Casarosa^{l,m}, L. Corona^{l,m},
5 T. Czank^q, S. B. Das^h, G. Dujany^e, C. Finck^e, F. Forti^{l,m}, M. Friedl^b,
6 A. Gabrielli^{n,o}, E. Ganiev^{n,o}, B. Gobbo^o, S. Halder^k, K. Hara^{s,p}, S. Hazra^k,
7 T. Higuchi^q, C. Irmiler^b, A. Ishikawa^{s,p}, H. B. Jeon^t, Y. Jin^{n,o}, C. Joo^q,
8 M. Kaleta^u, A. B. Kaliyar^k, J. Kandra^c, K. H. Kang^q, P. Kapusta^u,
9 P. Kodyš^c, T. Kohriki^s, M. Kumar^h, R. Kumarⁱ, C. La Licata^q, K. Lalwani^h,
10 R. Lebouchier^d, S. C. Lee^t, J. Libby^g, L. Martel^e, L. Massaccesi^{l,m},
11 S. N. Mayekar^k, G. B. Mohanty^k, T. Morii^q, K. R. Nakamura^{s,p},
12 Z. Natkaniec^u, Y. Onuki^r, W. Ostrowicz^u, A. Paladino^{l,m}, E. Paoloni^{l,m},
13 H. Park^t, L. Polat^d, K. K. Rao^k, I. Ripp-Baudot^e, G. Rizzo^{l,m}, D. Sahoo^k,
14 C. Schwanda^b, J. Serrano^d, J. Suzuki^s, S. Tanaka^{s,p}, H. Tanigawa^r,
15 R. Thalmeier^b, R. Tiwari^k, T. Tsuboyama^{s,p}, O. Verbycka^u, L. Vitale^{n,o},
16 K. Wan^r, Z. Wang^r, J. Webb^a, J. Wiechczynski^m, H. Yin^b, L. Zani^d,

17 (Belle-II SVD Collaboration)

18 ^a*School of Physics, University of Melbourne, Melbourne, Victoria 3010, Australia*

19 ^b*Institute of High Energy Physics, Austrian Academy of Sciences, 1050 Vienna, Austria*

20 ^c*Faculty of Mathematics and Physics, Charles University, 121 16 Prague, Czech Republic*

21 ^d*Aix Marseille Université, CNRS/IN2P3, CPPM, 13288 Marseille, France*

22 ^e*IPHC, UMR 7178, Université de Strasbourg, CNRS, 67037 Strasbourg, France*

23 ^f*Indian Institute of Technology Bhubaneswar, Satya Nagar, India*

24 ^g*Indian Institute of Technology Madras, Chennai 600036, India*

25 ^h*Malaviya National Institute of Technology Jaipur, Jaipur 302017, India*

26 ⁱ*Punjab Agricultural University, Ludhiana 141004, India*

27 ^j*Punjab University, Chandigarh 160014, India*

28 ^k*Tata Institute of Fundamental Research, Mumbai 400005, India*

29 ^l*Dipartimento di Fisica, Università di Pisa, I-56127 Pisa, Italy*

30 ^m*INFN Sezione di Pisa, I-56127 Pisa, Italy*

31 ⁿ*Dipartimento di Fisica, Università di Trieste, I-34127 Trieste, Italy*

32 ^o*INFN Sezione di Trieste, I-34127 Trieste, Italy*

33 ^p*The Graduate University for Advanced Studies (SOKENDAI), Hayama 240-0193, Japan*

34 ^q*Kavli Institute for the Physics and Mathematics of the Universe (WPI), University of*

35 *Tokyo, Kashiwa 277-8583, Japan*

36 ^r*Department of Physics, University of Tokyo, Tokyo 113-0033, Japan*

37 ^s*High Energy Accelerator Research Organization (KEK), Tsukuba 305-0801, Japan*

38 ^t*Department of Physics, Kyungpook National University, Daegu 41566, Korea*

39 ^u*H. Niewodniczanski Institute of Nuclear Physics, Krakow 31-342, Poland*

40 Abstract

41 The Silicon Vertex Detector (SVD) is a part of the vertex detector in the
42 Belle II experiment at the SuperKEKB collider (KEK, Japan). Since the start

43 of data taking in spring 2019, the SVD has been operating stably and reliably
44 with a high signal-to-noise ratio and hit efficiency, achieving good spatial resolu-
45 tion and high track reconstruction efficiency. The hit occupancy, which mostly
46 comes from the beam-related background, is currently about 0.5% in the in-
47 nermost layer, causing no impact on the SVD performance. In anticipation of
48 the operation at higher luminosity in the next years, two strategies to sustain
49 the tracking performance in future high beam background conditions have been
50 developed and tested on data. One is to reduce the number of signal waveform
51 samples to decrease dead time, data size, and occupancy. The other is to uti-
52 lize the good hit-time resolution to reject the beam background hits. We also
53 measured the radiation effects on the full depletion voltage, sensor current, and
54 strip noise caused during the first two and a half years of operation. The results
55 show no detrimental effect on the SVD performance.

56 *Keywords:* Silicon strip detector, Vertex detector, Tracking detector, Belle II

57 1. Introduction

58 The Belle II experiment [1] aims to probe new physics beyond the Standard
59 Model in high-luminosity e^+e^- collisions at the SuperKEKB collider (KEK,
60 Japan) [2]. The main collision energy in the center-of-mass system is 10.58 GeV
61 on the $\Upsilon(4S)$ resonance, which enables various physics programs based on the
62 large samples of B mesons, τ leptons, and D mesons. Also, the asymmetric en-
63 ergy of the 7 GeV e^- beam and 4 GeV e^+ beam is adopted for time-dependent
64 CP violation measurements. The target of SuperKEKB is to accumulate an in-
65 tegrated luminosity of 50 ab^{-1} with peak luminosity of about $6 \times 10^{35} \text{ cm}^{-2}\text{s}^{-1}$.
66 In June 2021, SuperKEKB recorded the world's highest instantaneous luminos-
67 ity of $3.1 \times 10^{34} \text{ cm}^{-2}\text{s}^{-1}$. The data accumulated before July 2021 corresponds
68 to an integrated luminosity of 213 fb^{-1} .

69 The Vertex Detector (VXD) is the innermost detector in the Belle II detector
70 system. The VXD has six layers: the inner two layers (layers 1 and 2) are the
71 Pixel Detector (PXD), and the outer four layers (layers 3 to 6) are the Silicon

72 Vertex Detector (SVD) [3]. The schematic cross-sectional view of the VXD is
 73 shown in Fig. 1. The PXD consists of DEPFET pixel sensors, and its innermost
 74 radius is 1.4 cm from the beam interaction point (IP). A detailed description of
 75 the SVD appears in Sec. 2.

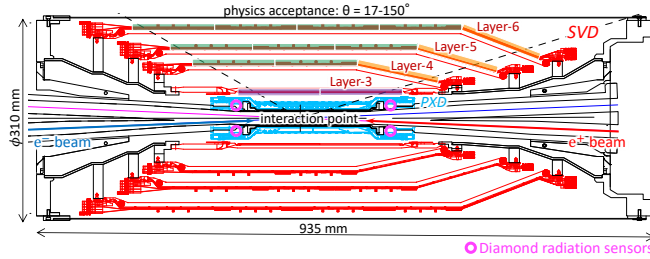


Figure 1: Schematic cross-sectional view of the VXD. The SVD is red, the PXD is light blue, and the IP beam pipe diamonds are pink circles. In the upper half of the VXD the locations of the three types of SVD DSSDs are indicated by boxes in three colors: purple for small sensors, green for large sensors, and orange for trapezoidal sensors as described in Tab. 1.

76 Diamond sensors [4] are mounted on the IP beam pipe and the bellows pipes
 77 outside of the VXD. The diamond monitors radiation doses for estimating the
 78 dose in the SVD. The diamond also sends beam abort requests to SuperKEKB
 79 to avoid severe damage to the detector if the radiation level gets too high.

80 2. Belle II Silicon Vertex Detector

81 The SVD is crucial for extrapolating the tracks to the PXD to measure the
 82 decay vertices with the PXD and point at a region-of-interest to reduce the PXD
 83 data. Other roles of the SVD are the standalone track reconstruction of low-
 84 momentum charged particles and their particle identification using ionization
 85 energy deposits. The SVD is also critical for vertexing the decay inside the
 86 SVD volume, i.e., long-lived particles like K_S mesons.

87 The SVD consists of four layers of double-sided silicon strip detectors (DSSDs) [5].
 88 The material budget of the SVD is about 0.7% of a radiation length per layer.
 89 On each DSSD plane, a local coordinate is defined with u -axis along n -side strips

90 and v -axis perpendicular to u -axis, i.e., p-side strips and n-side strips provide
 91 u and v information, respectively. In the cylindrical coordinate, u and v cor-
 92 responds to $r-\varphi$ and z . The SVD consists of three types of sensors: “small”
 93 rectangular sensors in layer 3, “large” rectangular sensors in the barrel region of
 94 layers 4, 5, and 6, and “trapezoidal” sensors installed slantwise in the forward
 95 region of layers 4, 5, and 6. The main characteristics of these sensors are sum-
 96 marized in Tab. 1. The sensors are manufactured by two companies: the small
 97 and large sensors by Hamamatsu and trapezoidal sensors by Micron. The full
 98 depletion voltage is 60 V for Hamamatsu sensors and 20 V for Micron sensors;
 99 both types of sensors are operated at 100 V.

| | Small | Large | Trapezoidal |
|-------------------|-------------------|-------------------|---------------------|
| No. of u/p-strips | 768 | 768 | 768 |
| u/p-strip pitch | 50 μm | 75 μm | 50–75 μm |
| No. of v/n-strips | 768 | 512 | 512 |
| v/n-strip pitch | 160 μm | 240 μm | 240 μm |
| Thickness | 320 μm | 320 μm | 300 μm |
| Manufacturer | Hamamatsu | | Micron |

Table 1: Table of the main characteristics of the three types of sensors. Only readout strips
 are taken into account for number of strips and strip pitch. All sensors have one intermediate
 floating strip between two readout strips.

100 The front-end ASIC, the APV25 [6], was originally developed for the CMS
 101 Silicon Tracker. The APV25 tolerates more than 100 Mrad of radiation. It has
 102 128 channels with a shaping time of about 50 ns. For the SVD, the APV25
 103 is operated in “multi-peak” data sampling mode, visualized in Fig. 2. The
 104 chip samples the height of the signal waveform with the 32 MHz clock (31 ns
 105 period) and stores each sample in an analog ring buffer. Since the bunch-crossing
 106 frequency is eight times faster than the sampling clock, the stored samples are
 107 not synchronous to the beam collision in contrast to CMS. In the present readout
 108 configuration (the six-samples mode), at every reception of the Belle II global
 109 Level-1 trigger, the chip reads out six successive samples stored in the buffers.

110 The six-samples mode offers a wide enough time window ($6 \times 31 \text{ ns} = 187 \text{ ns}$)
 111 to accommodate large timing shifts of the trigger. In preparation for operation
 112 with higher luminosity, where background occupancy, trigger dead-time, and the
 113 data size increase, we developed the three/six-mixed acquisition mode (mixed-
 114 mode). The mixed-mode is a new method to read out the signal samples from
 115 the APV25, in which the number of samples changes between three and six
 116 in each event, depending on the timing precision of the Level-1 trigger signal.
 117 For triggers with precise timing, three-samples data are read out with half time
 118 window and half data size compared to six-samples data, reducing the effects
 119 due to higher luminosity. This functionality was already implemented in the
 120 running system and confirmed by a few hours of smooth physics data taking.
 121 Before starting to use the mixed-mode, we assess the performance degradation
 122 due to the change of the acquisition mode. As the first step, the effect in the
 123 hit efficiency was evaluated as described in Sec. 3.

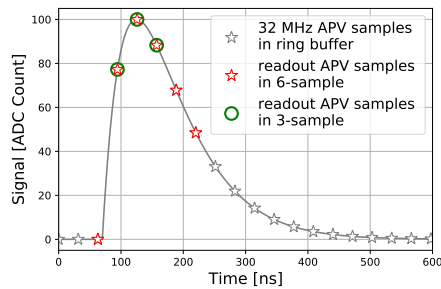


Figure 2: Example of sampling in “multi-peak” mode of the APV25. The gray line shows the signal waveform after the CR-RC shaper circuit. The stars show the sampled signal height recorded in the analog ring buffer according to the 32 MHz sampling clock. The red stars indicate the six successive samples read out at the trigger reception in the six-samples mode. The red stars with a green circle indicate the samples read out in the three-samples acquisition.

124 The APV25 chips are mounted on each middle sensor (chip-on-sensor con-
 125 cept) with thermal isolation foam in between. The merit of this concept is
 126 shorter signal propagation length and hence reduced noise level. To minimize
 127 the material budget the APV25 chips on the sensor are thinned down to 100 μm .

128 The APV25 chips are mounted on a single side of the sensor and the signal read-
129 out is performed from the opposite side via wrapped flexible printed circuits.
130 The power consumption of the APV25 chip is 0.4 W/chip and 700 W in the
131 entire SVD. The chips are cooled by a bi-phase -20°C CO_2 evaporative cooling
132 system.

133 **3. Performance**

134 The SVD has been operating reliably and smoothly since March 2019. The
135 total fraction of masked strips is about 1%. The only issue was the disable-
136 ment of one APV25 chip during the spring of 2019, which was remediated by
137 reconnecting a cable that summer. The SVD has also demonstrated stable and
138 excellent performance [7]. The hit efficiency is continuously over 99% in most of
139 the sensors. The charge collection is reasonably efficient, and the most probable
140 values of the cluster signal-to-noise ratio distributions range from 13 to 30.

141 We measured the cluster position resolution by analyzing the $e^+e^- \rightarrow \mu^+\mu^-$
142 data [8]. The resolution is estimated from the residual between the cluster po-
143 sition and the track position, not biased by the target cluster, after subtracting
144 the effect of the track extrapolation error. The cluster position resolutions for
145 different incident angles are shown in Fig. 3. The observed resolution has the
146 expected shape, showing a minimum when the tangent of the projected incident
147 angle equals strip pitch divided by sensor thickness. Given the various sensor
148 pitches with one floating strip, the minimum is expected at 14 (21) degrees on
149 the v/n-side and at 4 (7) degrees on the u/p-side for layer 3 (4, 5, and 6), respec-
150 tively. The resolution for normal incident angle is also in good agreement with
151 the expected digital resolution, that is 23 (35) μm on the v/n-side, 7 (11) μm
152 on the u/p-side, respectively for layer 3 (4, 5, and 6). Still, some studies are
153 ongoing to improve the resolution especially for the layer-3 u/p-side, where at
154 normal incidence a slightly higher resolution is measured (9 μm) compared to
155 the expectations.

156 The cluster hit-time resolution was also evaluated in candidate hadronic

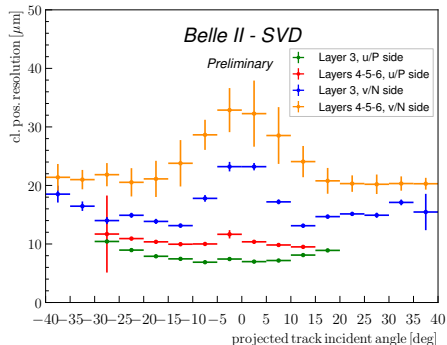


Figure 3: The SVD cluster position resolution depending on the projected track incident angle. The green (blue) plot shows the resolution in the u/p-side (n/v-side) of layer-3 sensors, and the red (yellow) one shows the u/p-side (n/v-side) of layers-4, 5, and 6 sensors.

157 events¹ using the reference event time estimated by the Central Drift Cham-
 158 ber (CDC) outside of the SVD. The error on the event time, about 0.7 ns,
 159 was subtracted to evaluate the intrinsic SVD hit-time resolution. The resulting
 160 resolution is 2.9 ns on the u/p-side and 2.4 ns on the v/n-side. The hit-time
 161 distributions for signal² and background³ are shown in Fig. 4. The narrowly
 162 peaking signal distribution and the broad background distribution make it pos-
 163 sible to reject off-time background hits efficiently. For example, if we reject
 164 hits with the hit-time less than -38 ns in this plot, we can reject 45% of the
 165 background hits while keeping 99% of the signal hits. The off-time hit rejection
 166 is essential to sustain the good tracking performance in the future high beam
 167 background condition.

168 To evaluate the performance in the mixed-mode, we compare three-samples
 169 data with six-samples data. The three-samples data shows comparable perfor-
 170 mance to the six-samples data for the trigger with no timing deviation because
 171 the three-sample's time window can accommodate the relevant part of the signal
 172 waveform to evaluate the signal height and timing. However, when the trigger

¹The events with more than three good tracks and not like Bhabha scattering.

²The clusters found to be used in the tracks in the hadronic events.

³The clusters in events triggered by delayed-Bhabha pseudo-random trigger.

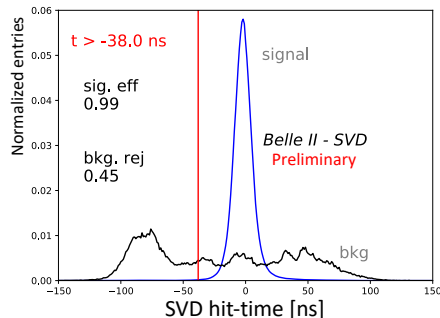


Figure 4: Example of the background hit rejection using hit-time. The blue distribution shows the signal, and the black distribution shows the background. The ordinates for signal and background are arbitrary normalized.

173 has a jitter and the timing shift happens, some part of the signal waveform can
 174 be out of the three-sample's time window, and the reconstruction performance
 175 deteriorates. We examined the effect on the hit efficiency as a function of the
 176 trigger timing shift. The effect is evaluated by the relative hit efficiency, which
 177 is defined as the ratio of the hit efficiency in the three-samples data to the one
 178 in the six-samples data. The trigger timing shift is evaluated by the CDC event
 179 time. For this study, the three-samples data are emulated in the offline analy-
 180 sis from the six-samples data by selecting consecutive three samples at a fixed
 181 latency to the Level-1 trigger signal. The resulting relative efficiencies as a func-
 182 tion of the trigger timing shift in the hadronic events are shown in Fig. 5. The
 183 decreasing trend is observed for the shift of the trigger timing, as expected. As
 184 a result, the relative efficiency is over 99.9% for the trigger timing shift within
 185 ± 30 ns, which is almost all the events.

186 4. Beam-related background effects on SVD

187 The beam-related background (BG) increases the hit occupancy of the SVD,
 188 which in turn degrades the tracking performance. To ensure the performance,
 189 we set the occupancy limit in layer-3 sensors to be about 3%, which will be
 190 loosened by a factor of two after we apply the hit-time rejection described in

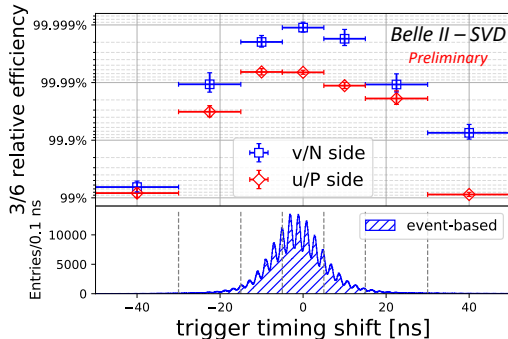


Figure 5: The relative hit efficiencies (the ratios of the hit efficiency in the three-samples data to the one in the six-samples data) as a function of the trigger timing shift for v/n-side (blue square) and u/p-side (red diamond). The positive (negative) trigger timing shift corresponds to early (late) trigger timing.

191 Sec. 3. Although the average hit occupancy in layer-3 sensors is below 0.5% with
 192 the current luminosity, it reaches about 3% in the projection at the luminosity
 193 of $8 \times 10^{35} \text{ cm}^{-2}\text{s}^{-1}$ based on the hit occupancy in the Monte Carlo (MC)
 194 simulation and the data/MC BG scale factors in the current beam optics.

195 Radiation effects in silicon sensors due to the BG are also relevant for the
 196 detector performance over the entire lifetime of the experiment. Surface dam-
 197 age is caused by ionizing energy loss, parameterized in terms of total ionizing
 198 dose. Effects due to bulk damage caused by displacement from non-ionizing
 199 energy loss (NIEL) are expressed as a function of the equivalent 1-MeV neutron
 200 fluence [9]. Bulk displacement damage from NIEL can alter the effective doping
 201 concentration and hence the depletion voltage, and can also increase the bulk-
 202 generated leakage current. Surface damage can lead to larger sensor capacitance
 203 and noise by increasing the SiO_2 fixed oxide charge, and higher surface-generated
 204 leakage current.

205 From the data/MC-rescaled BG extrapolation, the expected integrated dose
 206 in the SVD is about 0.2 Mrad/smy, and the equivalent 1-MeV neutron fluence
 207 is about $5 \times 10^{11} \text{ n}_{\text{eq}}/\text{cm}^2/\text{smy}$ (smy: Snowmass Year = 10^7 sec). The radiation
 208 hardness of the SVD sensors is about 10 Mrad and about $10^{13} \text{ n}_{\text{eq}}/\text{cm}^2$ based

209 on the irradiation campaigns on the SVD sensors [3], up to about 9 Mrad with
210 ^{60}Co source, and past studies relevant for the bulk damage on similar DSSD
211 sensors. Particularly relevant in this respect is the experience on the BaBar
212 Silicon Vertex Tracker, equipped with Micron DSSDs and exposed to similar
213 radiation as the SVD expectation. These sensors were successfully operated
214 for several years up to an integrated dose of 4.5 Mrad [10]. They were also
215 irradiated in dedicated campaigns to study bulk damage effects above bulk
216 type inversion (reached at about 3 Mrad of integrated dose and 10^{13}cm^{-2} of
217 equivalent neutron fluence), and operated successfully up to 9 Mrad [11, 12].
218 Considering these past studies, we expect to be able to safely operate the SVD
219 even for ten years at high luminosity, with a safety factor of two to three against
220 BG extrapolation. However, the long-term BG extrapolation is affected by large
221 uncertainties from the optimization of collimator settings in MC and the future
222 evolution of the non-simulated beam injection background. This uncertainty,
223 together with the relatively small safety factor, motivates the VXD upgrade to
224 improve the tolerance of hit rates and radiation damage, and the technology
225 assessment is ongoing for multiple sensor options.

226 In the first years of operation in Belle II, it is fundamental to carefully
227 monitor the integrated dose in the SVD and its effects on sensor properties,
228 such as depletion voltage, leakage current, and noise. Although not expected to
229 impact the detector performance, these initial measurements shown in the rest
230 of this section are crucial to confirm the extrapolation.

231 The integrated dose in the layer-3 mid-plane sensors, which are the most
232 exposed in the SVD, is estimated to be 70 krad in the first two and a half years
233 of operation. The estimation is based on the measured dose by the diamonds
234 on the IP beam pipe and the measured correlation between the SVD occupancy
235 and the diamond dose [13]. Thanks to a newly introduced random trigger line,
236 we removed an overestimation of factor three in the previous study. The new
237 estimate still has an uncertainty of about 50%, mainly due to the unavailability
238 of this new trigger line before December 2020. Assuming the dose/ n_{eq} fluence
239 ratio of $2.3 \times 10^9 n_{\text{eq}}/\text{cm}^2/\text{krad}$ from MC, 1-MeV equivalent neutron fluence is

240 evaluated to be about $1.6 \times 10^{11} \text{ n}_{\text{eq}}/\text{cm}^2$.

241 The full depletion voltage is measured from the relation between the v/n-side
242 strip noise and the bias voltage, as detailed in Ref. [7]. The result is consistent
243 with measurements performed on the bare sensors before the installation, rang-
244 ing from 20 to 60 V. No change in full depletion voltage is observed in the first
245 two and a half years of operation, as expected from low integrated neutron flu-
246 ence of $1.6 \times 10^{11} \text{ n}_{\text{eq}}/\text{cm}^2$ at this stage. This will be continuously monitored
247 since changes in the depletion voltage are expected in the future. After several
248 years with high luminosity, we could also observe bulk type inversion, at about
249 $10^{13} \text{ n}_{\text{eq}}/\text{cm}^2$, but from the experience on the BaBar DSSD reported above, we
250 expect no significant impact on our operation.

251 The leakage currents are generated in both bulk and surface, thus affected
252 by both ionizing and non-ionizing damage. The upper plot of Fig. 6 shows the
253 linear correlation between the current and the integrated dose. The slopes for
254 all the sensors are 2–5 $\mu\text{A}/\text{cm}^2/\text{Mrad}$, as summarized in the lower plot of Fig. 6.
255 The large variations can be explained by temperature effects and the deviation
256 from averaging the dose in each layer in the estimation. The slopes are in the
257 same order of magnitude as previously measured in the BaBar experiment [10],
258 1 $\mu\text{A}/\text{cm}^2/\text{Mrad}$ at 20°C. The precise temperature in layer 3 of the SVD is
259 unknown but expected to be in a similar regime. While the leakage current
260 is increasing, the impact on the strip noise is suppressed by the short shaping
261 time (50 ns) in APV25. It is expected to be comparable to the strip-capacitive
262 noise only after 10 Mrad irradiation and not problematic for ten years where
263 the integrated dose is estimated to be 2 Mrad.

264 The noise increases non-linearly to the integrated dose, as shown in Fig. 7.
265 The observed 20–25% increase in layer 3 does not affect the SVD performance.
266 Fixed oxide charges on sensor surface increase with dose, with saturation ex-
267 pected at around 100 krad, also non-linearly enlarging the inter-strip capaci-
268 tance. The noise saturation is already observed on the v/n-side and starts to
269 be seen on the u/p-side.

270 In conclusion, all the initial effects from radiation damage in the SVD mea-

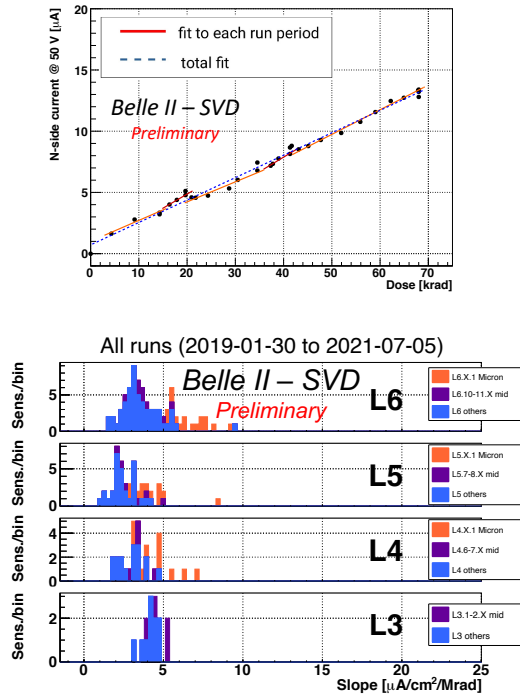


Figure 6: (upper) Effect of the integrated dose on the leakage current in the n/v-side of one layer-3 sensor. The slope is fitted for each run period (solid red line) and all the runs (dashed blue line). Both fit results agree with each other and are consistent with the linear increase. (lower) The fit results of all the sensors for all runs. The sensors are classified as trapezoidal sensors in the forward region (Micron), sensors around the midplane, and the others.

271 sured so far are within the expectation and do not affect detector performance.
 272 We expect good SVD performance can be kept after ten years with high lumi-
 273 nosity, with some safety margin on top of the extrapolation from BG simulation,
 274 affected by large uncertainty. A new irradiation campaign on the SVD sensors
 275 has also recently started to further study bulk damage effects even behind bulk
 276 type inversion.

277 5. Conclusions

278 The SVD has been taking data in Belle II since March 2019 smoothly and
 279 reliably. The detector performance is excellent and agrees with expectations.

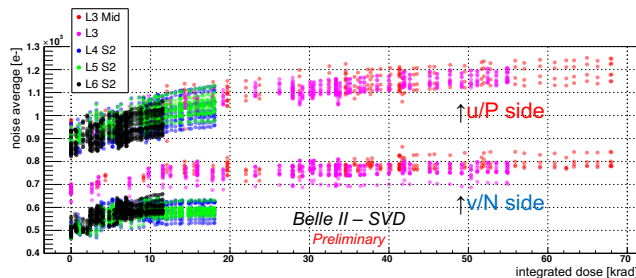


Figure 7: Effect of the integrated dose on the noise average in electron. The upper (lower) series shows the u/p-side (v/n-side) results, respectively.

280 We are ready to cope with the increased background during higher luminosity
 281 running by rejecting the off-time background hits using hit-time and operating
 282 in the three/six-mixed acquisition mode. In the recent study, the efficiency
 283 loss in the three-samples data is confirmed to be less than 0.1% for the trigger
 284 timing shift within ± 30 ns. The observed first effects of radiation damage are
 285 also within expectation and do not affect the detector performance.

286 Acknowledgments

287 This project has received funding from the European Union’s Horizon 2020
 288 research and innovation programme under the Marie Skłodowska-Curie grant
 289 agreements No 644294 and 822070. This work is supported by MEXT, WPI,
 290 and JSPS (Japan); ARC (Australia); BMBWF (Austria); MSMT (Czechia);
 291 CNRS/IN2P3 (France); AIDA-2020 (Germany); DAE and DST (India); INFN
 292 (Italy); NRF and RSRI (Korea); and MNiSW (Poland).

293 References

- 294 [1] T. Abe, et al., Belle II Technical Design Report (2010). arXiv:1011.0352.
 295 [2] Y. Ohnishi, et al., Accelerator design at SuperKEKB, Prog. Theor. Exp.
 296 Phys. 2013 (3), 03A011 (03 2013).

- 297 [3] K. Adamczyk, et al., The Design, Construction, Operation and Perfor-
298 mance of the Belle II Silicon Vertex Detector, to be submitted to J. In-
299 strument.
- 300 [4] S. Bacher, et al., Performance of the diamond-based beam-loss monitor
301 system of Belle II, Nucl. Instrum. Methods Phys. Res., Sect. A 997 (2021)
302 165157. arXiv:2102.04800.
- 303 [5] K. Adamczyk, et al., The Belle II silicon vertex detector assembly and
304 mechanics, Nucl. Instrum. Methods Phys. Res., Sect. A 845 (2017) 38–42,
305 proceedings of the Vienna Conference on Instrumentation 2016.
- 306 [6] M. J. French, et al., Design and results from the APV25, a deep sub-micron
307 CMOS front-end chip for the CMS tracker, Nucl. Instrum. Methods Phys.
308 Res., Sect. A 466 (2001) 359–365.
- 309 [7] G. Rizzo, et al., The Belle II Silicon Vertex Detector: Performance and
310 Operational Experience in the First Year of Data Taking, JPS Conf. Proc.
311 34 (2021) 010003.
- 312 [8] R. Leboucher, et al., Measurement of the cluster position resolution of the
313 Belle II Silicon Vertex Detector, these NIMA Conference Proceedings.
- 314 [9] G. Lindström, et al., 3rd RD48 status report, Tech. rep., CERN, Geneva
315 (Dec 1999).
- 316 [10] B. Aubert, et al., The BaBar detector: Upgrades, operation and perfor-
317 mance, Nucl. Instrum. Methods Phys. Res., Sect. A 729 (2013) 615–701.
- 318 [11] I. Rachevskaia, et al., Radiation damage of silicon structures with electrons
319 of 900MeV, Nucl. Instrum. Methods Phys. Res., Sect. A 485 (1) (2002) 126–
320 132.
- 321 [12] S. Bettarini, et al., Measurement of the charge collection efficiency after
322 heavy non-uniform irradiation in babar silicon detectors, in: IEEE Sympo-
323 sium Conference Record Nuclear Science 2004., Vol. 2, 2004, pp. 761–765
324 Vol. 2.

325 [13] L. Massaccesi, Performance study of the SVD detector of Belle II and future
326 upgrades, master thesis, Dipartimento di Fisica *E. Fermi*, Università di Pisa
327 (2021).
328 URL <https://docs.belle2.org/record/2759/>